APL Materials

Evidence for vacancy trapping in Au-hyperdoped Si following pulsed laser melting

Cite as: APL Mater. **7**, 101124 (2019); https://doi.org/10.1063/1.5124709
Submitted: 15 August 2019 . Accepted: 08 October 2019 . Published Online: 28 October 2019

W. Yang, N. Ferdous, P. J. Simpson, J. M. Gaudet, Q. Hudspeth, P. K. Chow, J. M. Warrender, A. J. Akey, M. J. Aziz, E. Ertekin, and J. S. Williams

ARTICLES YOU MAY BE INTERESTED IN

Multifold nodal points in magnetic materials
APL Materials **7**, 101125 (2019); https://doi.org/10.1063/1.5124314

Roadmap on material-function mapping for photonic-electronic hybrid neural networks
APL Materials **7**, 100903 (2019); https://doi.org/10.1063/1.5109689

Preparation and uses of large area single crystal metal foils
APL Materials **7**, 100905 (2019); https://doi.org/10.1063/1.5114861

© 2019 Author(s).

Evidence for vacancy trapping in Au-hyperdoped Si following pulsed laser melting

Cite as: APL Mater. 7, 101124 (2019); doi: 10.1063/1.5124709
Submitted: 15 August 2019 • Accepted: 8 October 2019 •
Published Online: 28 October 2019

View Online

Export Citation

CrossMark

W. Yang,[1] N. Ferdous,[2] P. J. Simpson,[3] J. M. Gaudet,[3] Q. Hudspeth,[4] P. K. Chow,[4] J. M. Warrender,[4] A. J. Akey,[5] M. J. Aziz,[5] E. Ertekin,[2] and J. S. Williams[1]

AFFILIATIONS

[1] Research School of Physics and Engineering, Australian National University, ACT 2601, Australia
[2] University of Illinois at Urbana-Champaign, Champaign, Illinois 61801, USA
[3] The University of Western Ontario, London, Ontario N6A 3K7, Canada
[4] U.S. Army ARDEC-Benét Laboratories, Watervliet Arsenal, New York 12189, USA
[5] Harvard John A. Paulson School of Engineering and Applied Sciences, Cambridge, Massachusetts 02138, USA

ABSTRACT

Nanosecond pulsed laser melting can be used to rapidly recrystallize ion-implanted Si through liquid phase epitaxy. The rapid resolidification that follows the melting results in a supersaturation of impurities and hyperdopes the Si, inducing novel optoelectronic properties with a wide range of applications. In this work, structural changes in the Si lattice in Au-hyperdoped Si are studied in detail. Specifically, we show that the local skewing of the lattice observed previously in regions of extremely high Au concentrations (>1.4 at. %) can be related to the displacement of Au from perfect lattice positions. Surprisingly, although the incorporation of the larger Au atoms into Si is expected to cause *swelling* of the lattice, reciprocal space mapping shows that a small amount (0.3 at. %) of lattice *contraction* (decrease in lattice parameter) is present in the hyperdoped layer. Furthermore, positron annihilation spectroscopy shows an elevated concentration of vacancies in the hyperdoped layer. Based on these observations and with the aid of density functional theory, we propose a phenomenological model in which vacancies are kinetically trapped into lattice sites around substitutional Au atoms during resolidification. This vacancy trapping process is hypothesized to occur as a means to minimize lattice strain and may be universal in pulsed laser melted Si systems.

© *2019 Author(s). All article content, except where otherwise noted, is licensed under a Creative Commons Attribution (CC BY) license (http://creativecommons.org/licenses/by/4.0/).* https://doi.org/10.1063/1.5124709

I. INTRODUCTION

Ion implantation followed by pulsed laser melting (PLM) is a well-known technique for incorporating impurities into Si, usually into substitutional lattice sites, at concentrations well in excess of the thermodynamic solubility limit.[1] This nonequilibrium process, known as *hyperdoping*, has been used to realize unique compositional and structural regimes in Si,[2,3] with diverse potential applications such as infrared photodetection,[4] intermediate band photovoltaics,[5] and superconductivity.[6] While hyperdoped Si has been shown to exhibit good crystalline quality, the local lattice environment is modified by high concentrations of impurity atoms that are often larger than Si (usually in the order of a few atomic percent). Lattice distortion and strain (normal to the surface) in hyperdoped layers are thus important to consider, especially as they could affect the optoelectronic properties of the material. However, there currently exists only a small body of literature on strain in pulsed laser melted Si, all of which has focused on conventional *n*- and *p*-type dopants (e.g., phosphorus and boron, respectively). A negative out-of-plane strain (lattice contraction) has been consistently measured for laser-melted Si hyperdoped with B, As, and Sb.[7–9] The latter two results are especially interesting, as the incorporation of As and Sb atoms should give rise to expansion of the lattice based on size considerations, since the covalent radii of both As (1.21 Å) and Sb (1.41 Å) are larger than the atomic radius of Si (1.17 Å).[10]

Two mechanisms have been proposed to explain the unexpected lattice contraction, although no consensus has been reached. Early work by Cargill *et al.*[11] attributed the lattice contraction measured in As-hyperdoped Si to the hydrostatic "electronic" strain associated with an increased number of free electrons in the

conduction band states. Later, in another study on As-hyperdoped Si, Parisini *et al.* showed that the lattice contraction scaled linearly with the carrier concentration, in accordance with the "electronic strain" model.[8] On the other hand, in a more recent density functional theory (DFT) study by Ahn and Dunham, it was argued that free electrons are actually expected to expand the lattice and that the unexpected negative strain measured is likely to have originated from high concentrations of vacancies in the form of As_mV_n clusters.[12] Incidentally, it is well known that As-V complexes are electrically inactive,[13] clearly indicating that the presence of vacancy clusters can affect electrical and potentially optical activity in hyperdoped Si. Armigliato *et al.* also hypothesized that the presence of a high concentration of vacancies could account for an anomalous high negative strain measured in Sb-hyperdoped Si.[9] Furthermore, Antonelli *et al.*[14] showed that isolated Si vacancies result in inward lattice relaxation. Thus, it is clear from the more recent studies that vacancies are the likely cause of the anomalous lattice contraction. Nonetheless, to date no direct experimental evidence has been reported to conclusively confirm the existence (or the lack thereof) of an enhanced population of vacancies in hyperdoped Si following PLM.

In this work, using Rutherford backscattering spectrometry combined with ion channeling (RBS/C), reciprocal space x-ray mapping (RSM), Doppler broadening positron annihilation spectroscopy (PAS), and density functional theory (DFT), the lattice distortion and local atomic environment in Si hyperdoped with a nonconventional dopant (i.e., Au) is investigated for the first time. We show that Au-hyperdoped Si exhibits a smaller out-of-plane lattice parameter compared with unstrained bulk Si and demonstrate how this contraction is directly related to the trapping of vacancies during resolidification following PLM. DFT shows that the structure of the Au-vacancy complex is akin to an Au interstitial in the middle of a divacancy, and that the inward attraction of Si atoms toward the defect results in a negative strain as observed by the experiment. We believe that the vacancy trapping process surrounding substitutional Au atoms occurs as a means of minimizing local lattice strain and may be a universal phenomenon for pulsed laser melted Si when incorporating larger impurity atoms.

II. METHODS

A. Experimental details

Samples were prepared by implanting 300 keV Au^+ ions into *n*-type, <100> oriented Si wafers (resistivity 1–10 Ω cm) to doses ranging from $2 - 6 \times 10^{15}$ cm^{-2} at the liquid nitrogen temperature. These implantation conditions are known[3] to give rise to a Au-rich amorphous layer of around 300 nm. A single pulse from a Nd:YAG laser was then used to melt the amorphous layer, with an energy density of ~0.8 J cm^{-2}. Previous characterization results detailed in Ref. 3 indicate that these conditions result in a hyperdoped layer of single crystalline Si with a peak Au concentration of 0.14–1.4 at. %. Excluding Au that has segregated onto the surface, the majority of the Au atoms have been incorporated into substitutional lattice positions, as measured by RBS/C. More detailed discussion on the segregation characteristics of these samples can be found in Ref. 3. We performed RBS/C with a 2 MeV He^+ beam and obtained angular scans about the three major channeling axes, namely, <100>, <110>, and <111>. The detector was situated at 78° from the sample normal for optimal depth resolution. The Si and Au yields presented here are integrated backscatter counts from the entire hyperdoped layer, excluding the surface Si and Au peaks.

Reciprocal space mapping was performed using a PANalytical X'Pert PRO system equipped with a rocking curves module containing a 3×Ge(220) monochromator and a CuKα_1 radiation source.

Positron annihilation spectroscopy uses a beam of monoenergetic positrons (0.2–16 keV) as a depth-resolved probe for voids, vacancies, surfaces, and electron density distribution of the sample of interest, from near-surface to a depth of about ~1.5 μm. The positron annihilates with a host electron, and two gamma rays of 511 keV are emitted in approximately opposite directions. The gamma rays are Doppler shifted by the momentum of the annihilated electron, and so the photopeak of their energy spectrum is broadened for annihilation with high-momentum electrons, such as those close to the ion cores. Where possible, positrons will seek regions far from the positively charged ion cores. This ensures that any voids or vacancies are over-represented in the spectrum. Meanwhile, electrons found in these regions tend to have lower momentum, resulting in narrower peaks. In the measurements performed for this study, the positron beam current is in the femto ampere range and a few times 10^5 events are analyzed using the *S*- (or sharpness) parameter.[13]

B. Computational methods

We simulated the gold-vacancy complex, Au-*V* in Si using DFT[15,16] as implemented in the Vienna *Ab initio* Simulation Package (VASP).[17,18] We used the Generalized Gradient Approximation-Perdew-Burke-Ernzerhof (GGA-PBE)[19] approximation for exchange/correlation, Projector-Augmented-Wave (PAW) method pseudopotentials,[20,21] and we considered spin polarized descriptions. Supercells containing 250 atoms (corresponding to an experimental defect concentration of 0.4 at. % for one defect per cell) are used with a Monkhorst-Pack *k*-mesh sufficient to converge total energies to within 0.01 eV. We use a plane wave basis set with 460 eV cutoff for orbital expansion, and atoms are relaxed until the total force on each atom is ≤0.01 eV/Å.

Defect formation energies $\Delta E_{D,q}$ are obtained as[22]

$$\triangle E_{D,q} = (E_{D,q} - E_{perf}) - \sum_i n_i \mu_i + q(E_v + E_F), \quad (1)$$

where $E_{D,q}$ is the total energy of a defect containing supercell, E_{perf} is the total energy of the supercell without any defect, n_i is number of added/removed ($n_i > 0/n_i < 0$) species *i* to form the defect, and μ_i is the chemical potential (*i* = Si, Au). The chemical potentials μ_{Au} and μ_{Si} were obtained from the elemental bulk phases to reflect Au- and Si-rich experimental conditions.

III. RESULTS AND DISCUSSION

A. Lattice distortion by Au

In the following discussion, we categorize our samples into two types:[3] (1) low concentration samples, which contain a laterally uniform Au concentration; and (2) high concentration samples, which contain laterally segregated, filamentary Au-rich regions (the concentration profile is also nonuniform in-depth and peaks at around 110 nm below the surface). The estimated local Au concentration

© Author(s) 2019

within the individual filamentary regions in the high concentration samples is >3 at. %. For Au-hyperdoped Si fabricated with an implantation energy of 300 keV, previous experimental results indicate that doses below 2×10^{15} cm^{-2} gave rise to "low concentration" behaviors, while doses above 3×10^{15} cm^{-2} resulted in "high concentration" behaviors.

Although our previous work established that most of the Au atoms are largely substitutional,[3] angular scans around the axial channels were found to be necessary to elucidate the displacement of the Au relative to perfect substitutional lattice positions. Figure 1 shows RBS spectra and angular channeling scans taken around the major axial channels on a sample that was implanted to 4×10^{15} cm^{-2} at 300 keV before PLM. Integration windows used to obtain the angular scans are shown in Fig. 1(a) and the Au profile prior to PLM is also shown in red to illustrate the segregation characteristics of Au after PLM (shown in black). It can be concluded that most of the Au is contained in the top 300 nm except for the 15% of the implanted Au dose that has segregated onto the surface. The width of the Si channels shown in Figs. 1(b)–1(d) is consistent with values obtained in the literature.[23] The dip in the Au yield in the middle of the Si channel is consistent with substitutional Au atoms occupying Si lattice sites. As the relative width of the Au dips (as compared with the respective Si dips) reflects the displacement of the Au atoms from lattice positions, the narrowing of the Au dips suggests that the larger Au atoms protrude slightly into the Si channels, an effect that is expected based on size considerations. However, the narrowing of the Au dip in the <110> direction is more prominent than in <100> and <111>. As summarized in Table I, while the narrowing in the FWHM of the Au dip is around 0.34° for both <100> and <111> channels, the narrowing in the <110> channel is much greater at 0.71°. This asymmetry indicates that the average atom site location of Au deviates somewhat from perfect substitutional lattice positions to directions with a significant component normal to the <110> axis. Angular scans taken on a sample that was implanted at 50 keV to a dose of 1×10^{15} cm^{-2} with a homogeneous Au concentration of <1 at. % (not shown) gave similar results.

It can thus be concluded that the presence of the Au, regardless of the homogeneity of the Au distribution, gives rise to a slight asymmetric displacement of Au atoms from perfect lattice positions. Indeed, our previous high resolution electron microscopy results,[3] taken on samples with high Au concentrations (>1.4 at. %) revealed lattice distortion around the Au-rich filaments. This lattice disorder is very local and does not extend beyond a few nanometers away from the filaments. We emphasize that the local distortion of the lattice does not correspond to the formation of Au nanoparticles or other secondary phases.[3] Note that in samples with a low and homogeneous Au distribution, the mass contrast is too small to be resolved by TEM.

TABLE I. FWHM of Au and Si dips in angular scans obtained from different crystalline axes for a sample subjected to a 300 keV Au-implant to 4×10^{15} cm^{-2} followed by PLM.

Channel	FWHM$_{Si}$ (deg)	FWHM$_{Au}$ (deg)	ΔFWHM (deg)
<100>	0.95	0.61	0.34
<110>	1.46	0.75	0.71
<111>	0.74	0.40	0.34

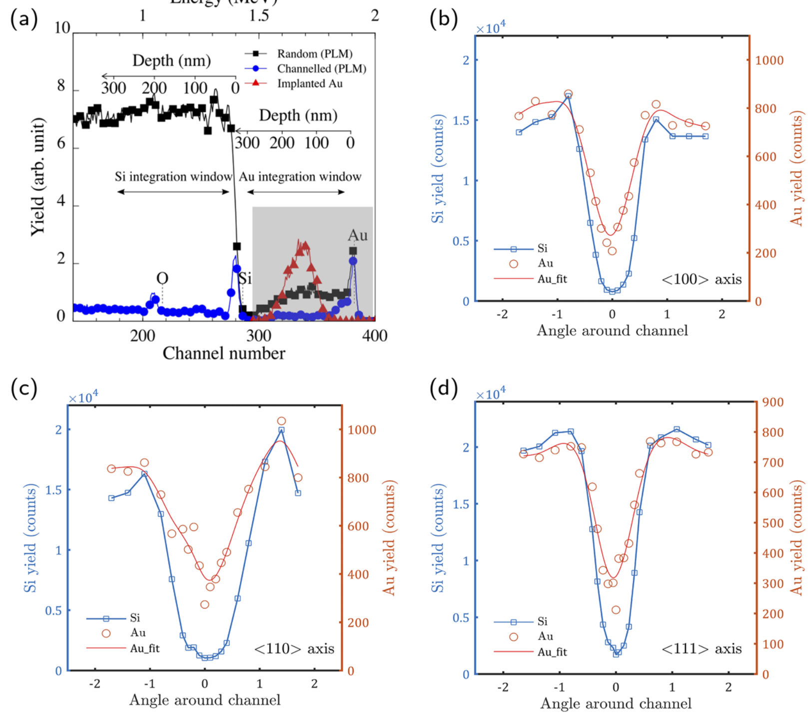

FIG. 1. (a) RBS/C spectra of the sample that is implanted to 4×10^{15} cm^{-2} outlining the integration windows for Au and Si. The Au part of a random spectrum taken on the sample prior to PLM shows the implanted Au profile. Note that for all spectra, the region highlighted in gray has been magnified by a factor of 2 for visual clarity. Angular scans taken (b) around the (100) axial channel, (c) around the (110) channel, and (d) around the (111) channel. Spline fits for the Au dips are shown for visual clarity. Further RBS/C measurements taken on this sample can be found elsewhere.[3]

© Author(s) 2019

Both the variation in the displacement of the Au from lattice positions and the lattice distortions seen previously in TEM are suggestive of lattice strain. We therefore employed reciprocal space mapping (RSM) to measure the lattice expansion/contraction. The out-of-plane lattice constant of the hyperdoped layer, $a_{\perp}$, is obtained from asymmetric RSM around the Si(113) reflection. As shown in Fig. 2, the diffuse satellite peak located to the upper left of the Si substrate peak can be attributed to the Au hyperdoped layer. In the case of the high concentration sample shown here, $a_{\perp}$ is found to be 5.413 Å, which corresponds to an out-of-plane strain value $\varepsilon_{Au} = -0.3\%$. However, reciprocal space maps on low concentration samples (not shown) did not produce any detectable satellite peaks, presumably because the average strain present, if any, is below the detection limit of the system.

The covalent radius of Au is 1.40 Å, larger than that of Si (1.17 Å).[10] Thus, based on Vegard's law,[24] the incorporation of Au in Si is expected to cause a swelling of the lattice, giving rise to an increase in the lattice parameter out-of-plane as the hyperdoped layer is constrained in-plane. Thus, the negative out-of-plane strain measured here cannot be reconciled based on size considerations alone and manifests with the same apparent contradiction as that reported for laser-melted As- and Sb-hyperdoped Si earlier.[8,9] Consequently, the negative strain measured here must have some contribution other than the size effect described by Vegard's law. Since vacancies have previously been proposed as the likely reason for lattice contraction in heavily Sb-doped Si,[9] we next used Doppler broadening positron annihilation spectroscopy to directly measure the presence of vacancies in Au-hyperdoped Si. We note that the presence of vacancy-type defects is also consistent with indirect measurements (perturbed angular correlations).[25]

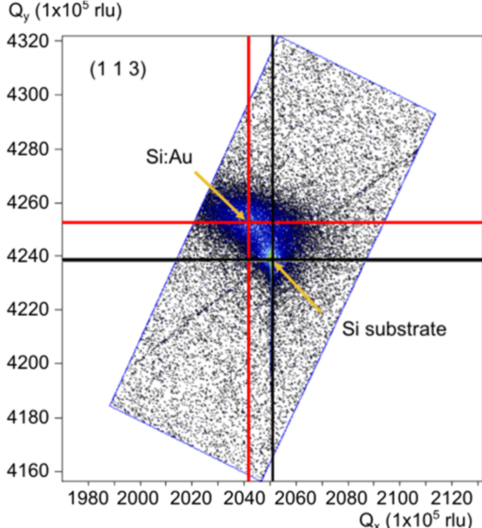

FIG. 2. Reciprocal space map around the Si(113) reflection, taken on a sample that has been implanted at 300 keV to a Au dose of 6×10^{15} cm^{-2} (a high concentration sample). The diffuse satellite peak in the upper left corner is associated with the Au-hyperdoped Si layer and indicates a decrease in the out-of-plane lattice parameter (negative strain).

B. Elevated vacancy concentration

Vacancy-type defects act as traps for diffusing positrons and the electronic environment of vacancies elevates the *S*-parameter. Thus, the *S*-parameter provides an estimate of vacancy concentration. The normalization of the *S*-parameter is performed by dividing the *S*-parameters at a depth by the *S*-parameter deep in the virgin Si bulk (obtained at a mean depth of ~1300 nm). Note that the positron distribution is broad and is spread out roughly from the surface to twice the mean depth, and so the *S*-parameter at 200 nm, say, is indeed the average value over 0–400 nm. In addition, the positron implantation profile becomes broader at greater implantation energies so that the *S*-parameter values at greater depths are averaged over a larger region. Furthermore, the diffusion of the positrons within the sample prior to annihilation tends to smear out the depth profile at all locations in the sample. This is seen most prominently in the influence of the surface (which has a small *S* value) on the first 400 nm of the bulk. Beyond the maximum diffusion length of positrons in Si, the *S*-parameter value is representative of the bulk.

Figure 3 shows the normalized PAS *S*-parameter for Au-hyperdoped Si samples as a function of the mean positron depth. Virgin Si shows a reduced *S*-parameter at the surface (up to a mean depth of 200 nm), an effect that is characteristic of the native oxide-silicon interface for low positron energy/depth, and rises asymptotically to a value characteristic of virgin bulk Si. Furthermore, a control Si sample which was ion implanted with Si^{28} at 110 keV (which produces an *a*-Si thickness of around 250 nm) and underwent the same PLM process resulted in identical *S*-parameters as

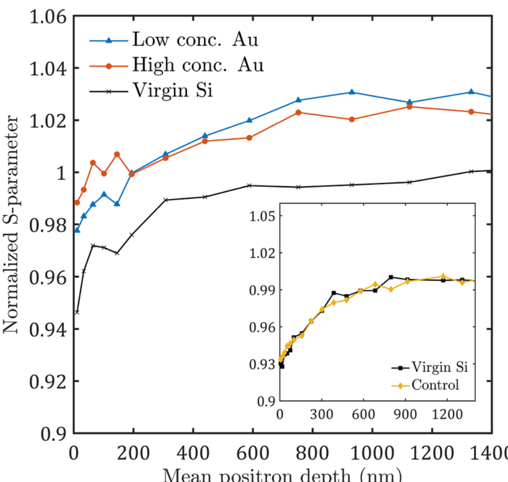

FIG. 3. *S*-parameter of the low and high concentration Au-hyperdoped samples (implanted to a dose of 2×10^{15} cm^{-2} and 6×10^{15} cm^{-2}, respectively) and a virgin Si sample, normalized with respect to the *S*-parameter value of bulk Si (obtained from the virgin Si sample at a mean depth of roughly 1300 nm) vs mean positron depth. Inset shows the normalized *S*-parameter of a virgin Si sample and a control sample made by Si self-implantation (110 keV, 2×10^{15} cm^{-2}) followed by identical PLM conditions as the Au-hyperdoped samples. The plotted *S*-parameter of the control sample is the numerical average of 3 independent measurements. We estimate that the absolute error in the normalized *S*-parameter is around ±0.005, although for reasons indicated in the text, this does not translate to the accuracy of any quantitative estimates of vacancy concentration.

© Author(s) 2019

the virgin Si, as shown in the inset.[26] This result is consistent with previous results,[13] unambiguously demonstrating that the enhanced vacancy concentration in the hyperdoped layer does not arise from the PLM process itself, but is rather associated with the incorporation of the Au atoms. On the other hand, both Au-hyperdoped Si samples show an elevated *S*-parameter. This result strongly suggests the presence of vacancy-type defects, although an accurate estimation of the vacancy concentration is not possible as the *S*-parameter is modified by the local electronic environment (local doping caused by Au) and is also sensitive to the large concentrations of Au atoms themselves. In the top ~400 nm, the *S*-parameter of the sample with a higher Au dose is higher than that of the low dose. Beyond the hyperdoped layer, the *S*-parameter becomes less dependent on the Au implantation dose. This indicates that the concentration of vacancies between the two samples are different within the Au-hyperdoped layer only. We note that the depth of damage apparent in the positron data (>1000 nm) for the Au-hyperdoped samples extends well beyond the depth expected from the implantation range (~300 nm), while the same effect is not observed on the self-implanted control sample (see Fig. 3, inset) that had undergone the same PLM process. Therefore, this difference is unlikely to be related to the ion-implantation or the PLM process. We speculate that an electric field induced by the *p*-type Au-hyperdoped layer[4] may have driven the positrons from the bulk (i.e., beyond the hyperdoped layer) toward the surface (i.e., into the hyperdoped layer), thus extending the apparent depth. Indeed, modeling by POSTRAP[27] shows that such an electric field is expected to produce the measured *S*-parameters. However, the modeling result is not conclusive as the simulated data are not unique; other models could also give rise to the same *S*-parameter data and further investigation is required.

In summary, our PAS results strongly support the presence of vacancies in Au-hyperdoped Si following PLM and that the vacancy concentration increases with Au concentration. However, we cannot reliably estimate the vacancy concentration as a function of depth due to electronic effects of the Au doping and other influences of high Au concentration on the measured *S*-parameter.

C. Au-*V* complexes

To determine how vacancies and Au atoms are incorporated in hyperdoped Si, and whether vacancies are expected to introduce a decrease in out-of-plane lattice parameter when trapped by the Au, we employed DFT to simulate the possible configuration of vacancies, Au atoms, and their interactions in Au-hyperdoped Si.

As shown in Fig. 4(a), we considered isolated vacancies trapped by a substitutional Au atom in nearest (*n*) and next nearest (*nn*) neighbor positions, respectively. Since the relaxation of atoms surrounding a Au_{Si} or vacancy may not be symmetrical, we considered both tetrahedral (T_d) and orthorhombic (C_{2v}) cases. For both symmetries considered, both *n* and *nn* relaxed into the same final configuration exhibiting trigonal (D_{3d}) symmetry. In this relaxed configuration, denoted Au_i-2V, Au sits in an interstitial position between two vacancies as shown in Fig. 4. Other possible configurations were also considered, but Au_i-2V was found to be the most energetically favorable with a total defect formation energy of 2.60 eV. The formation of Au_{Si}-V appears to be slightly more favorable with a large 2.64 eV binding energy compared to an isolated Au_{Si} and vacancy. This configuration is similar to that observed from a deep level

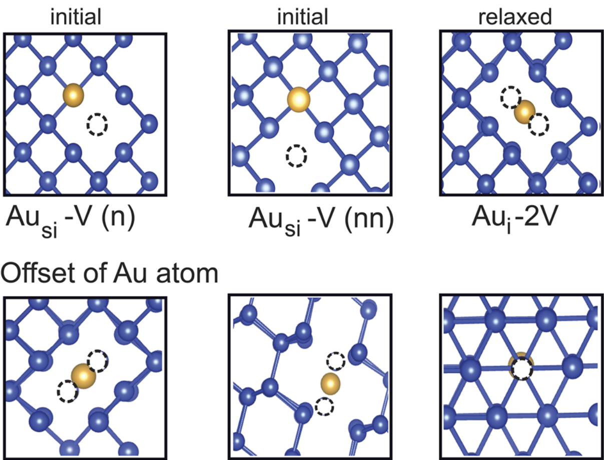

FIG. 4. (a) Possible Au-vacancy configurations in Si. Initial geometry of Au_{Si} with the nearest (*n*) neighbor vacancy, initial geometry of Au_{Si} with next nearest (*nn*) neighbor vacancy, and final relaxed geometry showing Au interstitial in the middle to two vacancies, Au_i–2V. Gold colored atoms are Au, blue colored atoms are Si and dotted black circles are the vacancies. (b) Offset of Au atoms from a regular Si lattice site in <100>, <110> and <111> directions. Dotted black circle shows the regular Si lattice sites which are now vacant.

transient spectroscopy (DLTS) study of a Au-vacancy complex[28] and electron paramagnetic resonance (EPR) studies for Sn-vacancy complexes,[29] where the impurity-vacancy pair can essentially be visualized as an impurity atom sitting in the middle of a divacancy. However, as we shall discuss below, the vacancy trapping process is likely to be a kinetic process as a result of the nonequilibrium nature of rapid solidification from the melt, and hence, may not be restricted by thermodynamic considerations. Thus, a variety of defects including Au_{Si},[30] isolated vacancies, and Au_i-2V, may be present in reality.

Nevertheless, the Au_i-2V complex is expected to give rise to local lattice contraction, consistent with RSM data shown above. It is seen from the relaxed geometry of Fig. 4(a) that the resulting Au_i-2V attracts the neighboring Si atoms inward. This pulling effect mostly increases the Si-Si bond length around the layer surrounding Au_i-2V. Table II shows the percentage elongation of local Si–Si bonds surrounding Au_i–2V as a function of the defect concentration, showing that higher Au_i–2V concentrations create more contraction in the lattice, consistent with experimental observations. The inward stretching causes the rest of the Si lattice encompassing the defect to be pulled inward, building tension in the surrounding host. Au atoms deviate the most from their regular lattice position when viewed from the <110> direction, compared to the other directions <100> and <111> as shown in Fig. 4(b), consistent with the direction-dependent deviation of Au atoms observed in the experiment. However, as we have established in Ref. 3, the distribution of Au is highly inhomogeneous within the hyperdoped layer, and thus the local bond elongation is expected to not only be inhomogeneous but also result in local differences in the nature of Au-V complexes across the hyperdoped layer. In addition, the

© Author(s) 2019

TABLE II. Calculated local Si–Si bond elongation expected for Au_i–2V at different Au concentrations.

Concentration of Au (at. %)	Local Si–Si bond elongation (%)
0.23	0.65
0.40	0.92
0.78	1.13

lattice contraction measured by XRD is actually the overall contraction in the entire hyperdoped layer. It is thus impossible to determine the concentration of vacancies required to produce the measured contraction (even if one assumes only one type of Au-V configuration, which is unlikely to be the case).

D. A vacancy trapping model

On the basis of the results shown above, we propose a phenomenological description of a vacancy trapping process that could occur during the resolidification of Si following PLM. The rapid resolidification traps a much higher concentration of substitutional Au atoms than that is possible in local interfacial equilibrium. As the covalent radius of Au is larger than that of Si, the incorporation of the Au strains the bonds nearby, as depicted in Fig. 4. As a self-compensating mechanism, we propose that vacancies are generated in the surrounding lattice (*n* and *nn*) during subsequent solidification at the retreating melt-solid interface, either by the migration of Si atoms away from their initial lattice positions, or through the injection of vacancies through the surface or at the melt-solid interface itself, to allow for the bond-rearrangement to minimize strain. As this process is kinetically limited by the moving solidification front, the actual location of the vacancy is expected to be statistically distributed rather than being limited by lowest free energy considerations (such as those used in DFT calculations under equilibrium). The resultant Au-vacancy complexes are, given the experimental data for other impurity-vacancy complexes (e.g., As-V, Sb-V), expected to be stable at room temperature.[29]

To further confirm that the trapping of vacancies is only possible at extremely fast resolidification speeds such as those facilitated by PLM, it would be ideally desirable to compare PLM-hyperdoped samples prepared by different near-equilibrium methods. Because of the high diffusivity of Au, however, a comparable concentration of substitutional Au cannot be achieved through solid phase epitaxy processes.[31] To this end, we note that, in a comparative study of Se-hyperdoped Si fabricated by flash lamp annealing and PLM, the Se-hyperdoped Si fabricated by PLM showed an unexplained secondary x-ray diffraction peak on the right-hand side of the main Si peak (suggestive of a smaller lattice parameter than pristine Si), while those fabricated by flash lamp annealing exhibited a larger lattice parameter as expected from the size difference between Se and Si.[32] These results are again consistent with the vacancy trapping model proposed in this study.

It is important to note that impurities such as As, Sb, and Al are known to form impurity-vacancy complexes at high concentrations when produced by equilibrium/near-equilibrium techniques such as LPCVD, cw-laser annealing (solid phase), and even Czochralski growth.[33–37] However, we point out that these impurity-vacancy complexes, which give rise to electrically inactive dopant clusters, are of a fundamentally different nature to the vacancies trapped following PLM. Indeed, *positive* strain has been reported by Pogany *et al.* and Takamura *et al.*[24,38] on heavily Sb-doped Si made by ion implantation followed by rapid thermal annealing and, in the latter study, laser melting with 10 successive shots, both of which would result in less nonequilibrium kinetic impurity trapping than one would expect from a single PLM shot. Such results are contrary to those obtained on Sb-hyperdoped Si melted with a single laser shot at similar Sb concentrations,[9] yet they are consistent with our Au-Si data and can be explained in terms of the vacancy trapping process that can take place during ultrarapid (nonequilibrium) resolidification following PLM. Similarly, the positive strain measured on heavily Ga-doped Si prepared by molecular beam epitaxy (MBE) could also be attributed to the near-equilibrium epitaxy process associated with MBE.[39] Based on these observations, we believe that vacancy trapping could be a unique phenomenon during the resolidification following PLM as a means of minimizing strain, and that this "freezing in" of vacancies is not facilitated by equilibrium or near-equilibrium solid phase epitaxy techniques. In addition, although we cannot rule out very small clusters of multiple Au atoms with or without associated vacancies since our current analysis techniques are unable to detect them; our previous high resolution TEM and lattice imaging[3] could not detect any high order Au clusters nor any early stages of Au precipitation. Nonetheless, in a recent thermal annealing study after PLM,[40] we show that there is a relaxation stage during the early stages of subsequent thermal annealing prior to Au precipitation that is likely to involve Au dimers and higher order Au complexes. Thus, although we cannot rule out small higher-order Au complexes directly after PLM, we believe that they would constitute a very small fraction of total Au atoms.

Finally, it is interesting to contemplate the implications of Au-V complexes on the optical and electrical activity of Au-hyperdoped Si. It could be speculated that Au-V complexes, like As- and Sb-V complexes, are electrically inactive in Si.[35,36] In terms of the optical activity, in a subsequent publication, we will show that some Au-V complexes are optically active, while others are not. On the other hand, it has been shown that substitutional Au in Si is optically active.[3,30] Thus, it would be expected that vacancy trapping reduces the overall optical activity of Au-hyperdoped Si, depending on the nature of the Au-V complexes.

IV. CONCLUSION

In conclusion, we have shown that Au atoms in hyperdoped Si fabricated using ion implantation and PLM reside on near-substitutional lattice sites but deviate slightly into the <110> axis and reduce the lattice parameter of Si slightly. Positron annihilation measurements reveal an enhanced concentration of vacancy-type defects in the hyperdoped Si, and DFT shows that the presence of Au-V complexes is consistent with the measured decrease in the out-of-plane lattice parameter. These results indicate that vacancies are trapped in Au-hyperdoped Si during the rapid resolidification of Si following PLM, resulting in local lattice contraction around the Au-V complexes. We believe that the trapping occurs as a means to minimize local lattice strain and may be a universal phenomenon in Si hyperdoped with large-size impurities by PLM.

© Author(s) 2019

ACKNOWLEDGMENTS

Funding from the U.S. Army under Contract No. FA5209-16-P-0104 is acknowledged for partial support of this work. We acknowledge access to NCRIS facilities (ANFF and the Heavy Ion Accelerator Capability). This work was performed in part at the Center for Nanoscale Systems (CNS), a member of the National Nanotechnology Coordinated Infrastructure Network (NNCI), which is supported by the National Science Foundation under NSF Award No. 1541959. CNS is part of Harvard University.

REFERENCES

[1] *Laser Annealing of Semiconductors*, edited by J. M. Poate and J. W. Mayer (Academic Press, 1982).
[2] A. J. Akey, D. Recht, J. S. Williams, M. J. Aziz, and T. Buonassisi, "Single-phase filamentary cellular breakdown via laser-induced solute segregation," Adv. Funct. Mater. **25**, 4642–4649 (2015).
[3] W. Yang, A. J. Akey, L. A. Smillie, J. P. Mailoa, B. C. Johnson, J. C. McCallum, D. Macdonald, T. Buonassisi, M. J. Aziz, and J. S. Williams, "Au-rich filamentary behavior and associated subband gap optical absorption in hyperdoped Si," Phys. Rev. Mater. **1**, 074602 (2017).
[4] J. P. Mailoa, A. J. Akey, C. B. Simmons, D. Hutchinson, J. Mathews, J. T. Sullivan, D. Recht, M. T. Winkler, J. S. Williams, J. M. Warrender, P. D. Persans, M. J. Aziz, and T. Buonassisi, "Room-temperature sub-band gap optoelectronic response of hyperdoped silicon," Nat. Commun. **5**(1), 3011 (2014).
[5] E. Antolin, A. Marti, J. Olea, D. Pastor, G. Gonzalez-Diaz, I. Martil, and A. Luque, "Lifetime recovery in ultrahighly titanium-doped silicon for the implementation of an intermediate band material," Appl. Phys. Lett. **94**, 042115 (2009).
[6] E. Bustarret, C. Marcenat, P. Achatz, J. Kačmarčik, F. Lévy, A. Huxley, L. Ortéga, E. Bourgeois, X. Blase, D. Débarre, and J. Boulmer, "Superconductivity in doped cubic silicon," Nature **444**, 465 (2006).
[7] B. R. Appleton, B. C. Larson, C. W. White, J. Narayan, S. R. Wilison, and P. P. Pronko, "New materials properties achievable by ion implantation and laser processing," AIP Conf. Proc. **50**, 291–298 (1979).
[8] A. Parisini, A. Bourret, A. Armigliato, M. Servidori, S. Solmi, R. Fabbri, J. R. Regnard, and J. L. Allain, "Electrical activity and structural evolution correlations in laser and thermally annealed As-implanted Si specimens," J. Appl. Phys. **67**, 2320–2332 (1990).
[9] A. Armigliato, F. Romanato, A. Drigo, A. Carnera, C. Brizard, J. R. Regnard, and J. L. Allain, "Anomalous low-temperature dopant diffusivity and defect structure in Sb- and Sb/B-implanted annealed silicon samples," Phys. Rev. B **52**, 1859–1873 (1995).
[10] J. G. Speight, *Lange's Handbook of Chemistry*, 16th ed. (McGraw-Hill Education, 2005).
[11] G. S. Cargill III, J. Angilello III, and K. L. Kavanagh, "Lattice compression from conduction electrons in heavily doped Si:As," Phys. Rev. Lett. **61**, 1748 (1988).
[12] C. Ahn and S. T. Dunham, "Charge carrier induced lattice strain and stress effects on As activation in Si," Appl. Phys. Lett. **93**, 022112 (2008).
[13] D. W. Lawther, U. Myler, P. J. Simpson, P. M. Rousseau, P. B. Griffin, and J. D. Plummer, "Vacancy generation resulting from electrical deactivation of arsenic," Appl. Phys. Lett. **67**, 3575 (1995).
[14] A. Antonelli, E. Kaxiras, and D. J. Chadi, "Vacancy in silicon revisited: Structure and pressure effects," Phys. Rev. Lett. **81**, 2088–2091 (1998).
[15] P. Hohenberg and W. Kohn, "Inhomogeneous electron gas," Phys. Rev. **136**, B864 (1964).
[16] W. Kohn and L. J. Sham, "Self-consistent equations including exchange and correlation effects," Phys. Rev. **140**, A1133 (1965).
[17] G. Kresse and J. Hafner, "*Ab initio* molecular dynamics for liquid metals," Phys. Rev. B **47**, 558 (1993).
[18] G. Kresse and J. Furthmüller, "Efficient iterative schemes for *ab initio* total-energy calculations using a plane-wave basis set," Phys. Rev. B **54**, 11169 (1996).
[19] J. P. Perdew, K. Burke, and M. Ernzerhof, "Generalized gradient approximation made simple," Phys. Rev. Lett. **77**, 3865 (1996).
[20] G. Kresse and D. Joubert, "From ultrasoft pseudopotentials to the projector augmented-wave method," Phys. Rev. B **59**, 1758 (1999).
[21] P. E. Blöchl, "Projector augmented-wave method," Phys. Rev. B **50**, 17953 (1994).
[22] S. B. Zhang and J. E. Northrup, "Chemical potential dependence of defect formation energies in GaAs: Application to Ga self-diffusion," Phys. Rev. Lett. **67**, 2339–2342 (1991).
[23] *Ion Beams for Materials Analysis*, edited by R. C. Bird and J. S. Williams (Elsevier Science, 1990).
[24] Y. Takamura, A. Vailionis, A. F. Marshall, P. B. Griffin, and J. D. Plummer, "Dopant deactivation in heavily Sb doped Si (001): A high-resolution x-ray diffraction and transmission electron microscopy study," J. Appl. Phys. **92**, 5503–5507 (2002).
[25] G. J. Kemerink and F. Pleiter, "Indium-vacancy interaction in laser-annealed silicon," Phys. Lett. A **121**, 367–370 (1987).
[26] Note that the two samples shown in the inset are measured with a slightly different electronic setup than the other samples, thus, producing a different shape.
[27] G. Aers, "Defect profiling in multilayered systems using mean depth scaling," in *Positron Beams for Solids and Surfaces*, edited by P. Schultz, P. J. Massoumi, and G. R. Simpson (AIP, New York, 1991), pp. 162–218.
[28] K. S. Koteswara Rao, V. Kumar, S. K. Premachandran, and K. P. Raghunath, "Interaction of gold-related and irradiation-induced defects in silicon," J. Appl. Phys. **69**, 8205–8209 (1991).
[29] G. D. Watkins, "Intrinsic defects in silicon," Mater. Sci. Semicond. Process. **3**, 227–235 (2000).
[30] N. Ferdous and E. Ertekin, "Atomic scale origins of sub-band gap optical absorption in gold-hyperdoped silicon," AIP Adv. **8**, 055014 (2018).
[31] W. Yang, S. Zhou, and J. S. Williams, "Comparison of Au trapping in Si fabricated by rapid thermal annealing, ion beam induced epitaxy, flash lamp annealing and pulsed laser melting" (unpublished).
[32] S. Zhou, F. Liu, S. Prucnal, K. Gao, M. Khalid, C. Baehtz, M. Posselt, W. Skorupa, and M. Helm, "Hyperdoping silicon with selenium: Solid vs. liquid phase epitaxy," Sci. Rep. **5**, 8329 (2015).
[33] G. Borot, L. Rubaldo, L. Clement, R. Pantel, D. Dutartre, K. Kuitunen, J. Slotte, F. Tuomisto, X. Mescot, M. Gri, and G. Ghibaudo, "Tensile strain in arsenic heavily doped Si," J. Appl. Phys. **102**, 103505 (2007).
[34] S. Kilpeläinen, K. Kuitunen, J. Slotte, F. Tuomisto, G. Borot, L. Rubaldo, L. Clément, R. Pantel, and D. Dutartre, "Defect characterization of heavily As and P doped Si epilayers," Phys. Status Solidi C **6**, 2537–2539 (2009).
[35] K. Saarinen, J. Nissilä, H. Kauppinen, M. Hakala, M. J. Puska, P. Hautojärvi, and C. Corbel, "Identification of vacancy-impurity complexes in highly *n*-type Si," Phys. Rev. Lett. **82**, 1883–1886 (1999).
[36] P. M. Voyles, D. J. Chadi, P. H. Citrin, D. A. Muller, J. L. Grazul, P. A. Northrup, and H. J. Gossmann, "Evidence for a new class of defects in highly *n*-doped Si: Donor-pair-vacancy-interstitial complexes," Phys. Rev. Lett. **91**, 125505 (2003).
[37] A. Chantre, "Defects in ultrafast quenched aluminum-doped silicon," Appl. Phys. Lett. **46**, 263–265 (1985).
[38] A. P. Pogany, T. Preuss, K. T. Short, H. K. Wagenfeld, and J. S. Williams, "Metastable solid solutions of antimony in (100) silicon," Nucl. Instrum. Methods Phys. Res. **209-210**, 731–736 (1983).
[39] K. L. Kavanagh and G. S. Cargill, "Lattice strain from substitutional Ga and from holes in heavily doped Si:Ga," Phys. Rev. B **45**, 3323–3331 (1992).
[40] W. Yang, Q. Hudspeth, P. K. Chow, J. M. Warrender, N. Ferdous, E. Ertekin, G. Malladi, A. J. Akey, M. J. Aziz, and J. S. Williams, "Atomistic mechanisms for the thermal relaxation of Au-hyperdoped Si," Phys. Rev. Appl. **12**, 024015 (2019).

© Author(s) 2019